

# Thickness-Dependently Enhanced Photodetection Performance of Vertically Grown SnS<sub>2</sub> Nanoflakes with Large Size and High Production

Xiansheng Jia,<sup>†,§</sup> Chengchun Tang,<sup>\*,†</sup> Ruhao Pan,<sup>†,‡</sup> Yunze Long,<sup>§</sup> Changzhi Gu,<sup>\*,†,‡</sup> and Junjie Li<sup>\*,†,‡</sup>

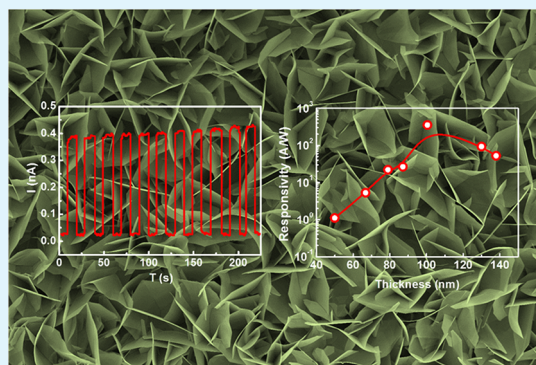
<sup>†</sup>Beijing National Laboratory for Condensed Matter Physics, Institute of Physics, Chinese Academy of Sciences, Beijing 100190, China

<sup>‡</sup>School of Physical Sciences, CAS Key Laboratory of Vacuum Physics, University of Chinese Academy of Sciences, Beijing 100049, China

<sup>§</sup>Collaborative Innovation Center for Nanomaterials & Optoelectronic Devices, College of Physics, Qingdao University, Qingdao 266071, China

**ABSTRACT:** Photodetection based on two-dimensional (2D) SnS<sub>2</sub> has attracted growing interest due to its superiority in response rate and responsivity, but high-quality growth and high performance photodetection of 2D SnS<sub>2</sub> still face great challenges. Here, high-quality SnS<sub>2</sub> nanoflakes with large-size and high-production are vertically grown on an Si substrate by a modified CVD method, having an average size of 30 μm with different thicknesses. Then a single SnS<sub>2</sub> nanoflake-based phototransistor was fabricated to obtain a high current on/off ratio of 10<sup>7</sup> and excellent performance in photodetection, including fast response rates, low dark current, and high responsivity and detectivity. Specifically, the SnS<sub>2</sub> nanoflakes show thickness-dependent photodetection capability, and a highest responsivity of 354.4 A W<sup>-1</sup> is obtained at the average thickness of 100.5 nm. A sensitized process using an HfO<sub>2</sub> nanolayer can further enhance the responsivity up to 1922 A W<sup>-1</sup>. Our work provides an efficient path to select SnS<sub>2</sub> crystal samples with the optimal thickness as promising candidates for high-performance optoelectronic applications.

**KEYWORDS:** tin sulfide, chemical vapor deposition, 2D materials, photodetector



## INTRODUCTION

Since the celebrated discovery of graphene, there has been growing interest in two-dimensional (2D) materials because they can display extraordinary properties in many fields.<sup>1</sup> Today monolayers of various types of layered materials can be synthesized using bottom-up and top-down approaches, and unprecedented physicochemical properties can be engineered by controlling the number of layers of 2D materials.<sup>2</sup> 2D layered metal dichalcogenides (MDCs) with the general formula of YX<sub>2</sub> are formed by a metal atom (Mo, W, Ga, Sn, etc.) sandwiched between two chalcogen layers (S, Se, Te). Since graphene is a zero-band gap semiconductor, it has traditionally had limited applications in electronic or photoelectronic devices. 2D MDC semiconductors have been considered to be suitable candidates for electronics or photoelectronics applications. SnS<sub>2</sub> is a member of the 2D MDC semiconductors with a hexagonal CdI<sub>2</sub> type crystal structure ( $a = 0.3648$  nm,  $c = 0.5899$  nm, space group  $P\bar{3}m1$ ) and an indirect band gap of 2.2 eV.<sup>3,4</sup> In recent studies, SnS<sub>2</sub> has exhibited good performance in many applications such as lithium ion batteries,<sup>5,6</sup> visible-light-driven photocatalysts,<sup>7,8</sup> field-effect transistors,<sup>9,10</sup> sensors,<sup>11,12</sup> and photodetec-

tors.<sup>4,13–16</sup> In particular, when SnS<sub>2</sub> nanoflakes were used as a photodetector, they showed superior performance such as fast response rate, high on/off ratio, high responsivity, and good stability. Furthermore, SnS<sub>2</sub>, as an earth-abundant and environmentally friendly material, is promising for practical or commercial applications.

Recently the growth of SnS<sub>2</sub> with high quality and efficiency has attracted much attention. Several methods, including exfoliation,<sup>17</sup> the solvothermal method,<sup>18</sup> atomic layer deposition (ALD),<sup>19</sup> and chemical vapor deposition (CVD),<sup>20</sup> have been reported to prepare 2D SnS<sub>2</sub> crystals. However, these methods also show some problems in controlling the size, thickness, yield, and uniformity of SnS<sub>2</sub> products. The exfoliation of bulk materials is low-producing and cannot prepare large-size thin 2D SnS<sub>2</sub> crystals with high uniformity. The solvothermal method needs a long reaction time and complex reaction and washing steps. The crystal size of SnS<sub>2</sub> deposited by ALD is too small for transfer and practical

**Received:** February 23, 2018

**Accepted:** May 10, 2018

**Published:** May 10, 2018

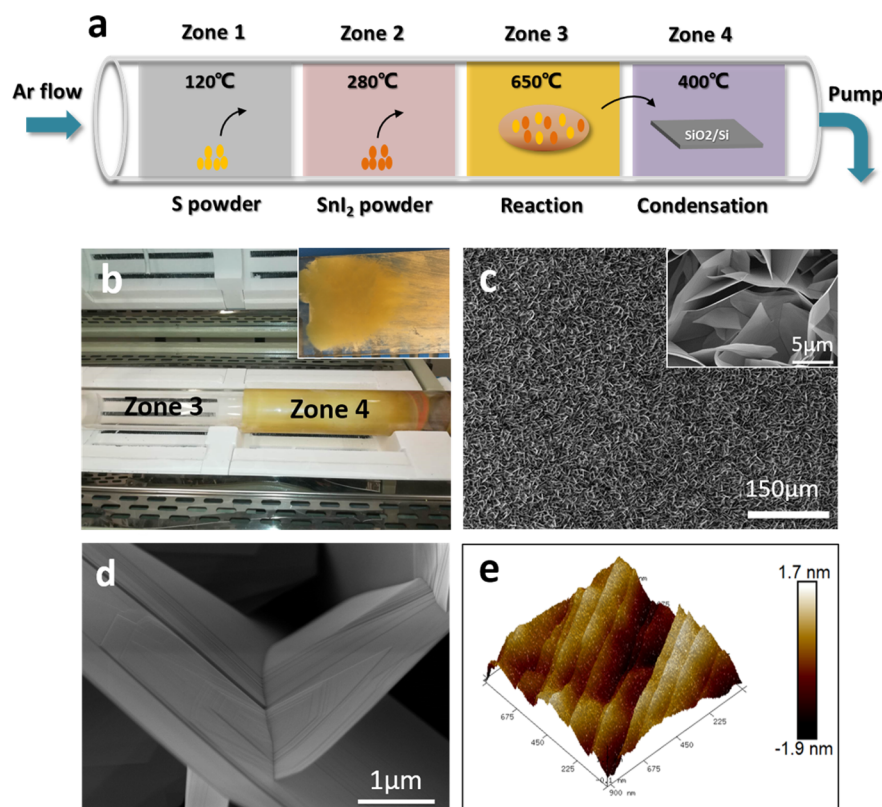


**Figure 1.** (a) Schematic illustration of a CVD system with four temperature zones for the growth of 2D SnS<sub>2</sub> crystal samples. (b) Photographs of Zone 4 and an inset of a sample, among yellow parts that indicate the SnS<sub>2</sub> flakes with high-density and production. (c) SEM image of large-area as-grown SnS<sub>2</sub> nanoflakes and enlarged SEM image of large-scale SnS<sub>2</sub> nanoflakes as an inset. (d) A high-resolution SEM image of a single flake shows the step-shaped morphology on the surface, which can be verified by AFM testing (e).

application. The CVD method is an appropriate method to prepare large-size thin 2D SnS<sub>2</sub> crystals. Su et al.<sup>13</sup> have reported for the first time the controlled CVD synthesis of a thin crystal array SnS<sub>2</sub> at the predefined location on SiO<sub>2</sub>/Si substrates. But the fabrication of an engineering nucleation site by the nanofabrication process increases the time and cost and may cause impurity in the as-prepared sample. And other reported CVD methods also meet with the same problem in attempting high-efficiency and high-production 2D SnS<sub>2</sub> crystals. Thus, the CVD growth of the 2D SnS<sub>2</sub> crystal needs further improvement to obtain high-quality 2D SnS<sub>2</sub> crystals for large-scale industrial device applications. Moreover, the optoelectronic properties of SnS<sub>2</sub> nanosheet-based photodetectors have been reported to exhibit significant application potential, but there are some flaws, such as low responsivities or long response time, which have rendered them inappropriate for current practical application. And thus both the growth and the performance of 2D SnS<sub>2</sub> crystals still need greatly to be improved.

Here, a simple and high-efficiency modified CVD method, including 4 different reactive areas, was used to prepare a vertically aligned 2D SnS<sub>2</sub> crystal nanoflake with high production and quality. The SnS<sub>2</sub> nanoflake-based photodetectors are fabricated to exhibit fast response rate, low dark current, large on/off ratio when exposed to light with really low power density, high responsivity, and detectivity. By measuring the photoresponsivities of SnS<sub>2</sub> nanoflakes with different thicknesses, an increasing trend of responsivities with an increase of average thickness from 50 to 100.5 nm has been found, and a highest responsivity of 354.4 A W<sup>-1</sup> and EQE of

$1.1 \times 10^5$  % can be contained. But the responsivities no longer increase when the thickness is more than 100.5 nm. Further, an effective sensitization process using HfO<sub>2</sub> film can greatly enhance the responsivity of the SnS<sub>2</sub> nanoflake-based photodetector to reach up to 1922 A W<sup>-1</sup>. Our works provide a modified CVD method to obtain high-production and high-quality SnS<sub>2</sub> nanoflake samples, finding the thickness-dependent photodetection capability of SnS<sub>2</sub> nanoflakes, which can be a promising candidate for fast and high-efficiency photodetector applications.

## EXPERIMENTAL SECTION

**Materials Preparation.** Tin iodide (SnI<sub>2</sub>, 99%) powder and sulfur (S, 99.5%) powder were obtained from Sinopharm Chemical Reagent Corp. Ltd., China. All the chemicals used in this study were used as-received without further purification.

**Sample Synthesis.** SnS<sub>2</sub> nanoflakes were synthesized via a chemical vapor deposition method with accurate temperature control by a tube furnace with four independent temperature control zones. 2.0 g S powder and 0.15g SnI<sub>2</sub> powder were used as source and placed in a quartz plate located in the first temperature zone and second temperature zone with the temperature at 120 °C and 280 °C, respectively. The third temperature control zone was used as a reaction zone with the temperature at 650 °C, in which SnI<sub>2</sub> steam and S steam react. The fourth temperature control zone was set as the deposition zone with the temperature at 400 °C. I<sub>2</sub> remained gaseous at 400 °C and SnS<sub>2</sub> was deposited into substrates located in the quartz tube. The holding time of the above temperature is 1 h. During the growth process, high-purity Ar with a flow rate of 50 sccm was used as the carrier gas. There were no reducing gases used as auxiliaries in the growth of SnS<sub>2</sub>.

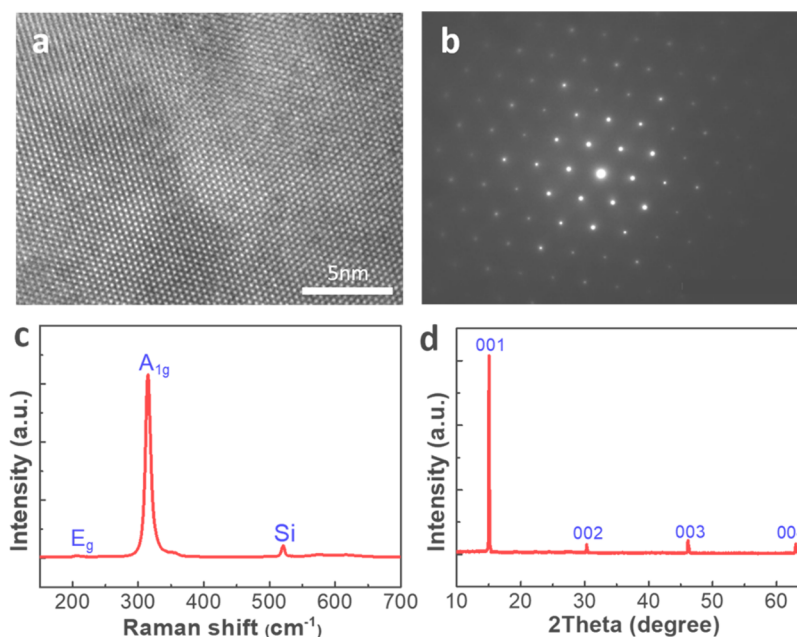


**Figure 2.** (a) HRTEM image of a select area of a single SnS<sub>2</sub> nanoflake, and (b) SAED pattern of the SnS<sub>2</sub> crystal. (c) Raman spectrum of SnS<sub>2</sub> crystals, exhibiting two typical peaks assigned to A<sub>1g</sub> and E<sub>g</sub>. (d) X-ray diffraction characterization of as-grown SnS<sub>2</sub> nanoflakes.

**Characterization.** The crystallinity of the as-synthesized SnS<sub>2</sub> nanoflakes was investigated using an X-ray diffractometer (XRD, PDPW3040/60) with a  $2\theta$  range of  $10^{\circ}$ – $65^{\circ}$  and Raman spectroscopy measurement (HR-800) with a wavenumber  $150$ – $700$   $\text{cm}^{-1}$ . The morphology and crystal structure of the as-prepared SnS<sub>2</sub> nanoflakes were characterized by field emission scanning electron microscopy (SEM, Helios 600i) and transmission electron microscopy (TEM, JEM2010). The thickness of the SnS<sub>2</sub> nanoflake was confirmed using atomic force microscopy (AFM, SPA-400).

**Fabrication and Measurement of SnS<sub>2</sub> Nanoflake-Based Photodetector.** The SnS<sub>2</sub> nanoflakes on Si substrate were dispersed in alcohol with ultrasound for about 3 s. A few drops of dispersion liquid were dropped onto the SiO<sub>2</sub>/Si substrate and were dried by nitrogen blowing to obtain in-plane oriented SnS<sub>2</sub> nanoflakes. Then the SiO<sub>2</sub>/Si substrate with SnS<sub>2</sub> nanoflakes was coated onto a 200 nm PMMA thin film as the photoresist by spin coating. The electrode patterns on the sides of the SnS<sub>2</sub> nanoflakes were contained by electron beam lithography (EBL, JBX-6300FS), and the Au/Cr electrodes were deposited by electron beam evaporation (EBE, Peva-600E). The photoresist was removed, and the SnS<sub>2</sub> nanoflake-based photodetectors were fabricated. The sensitization of SnS<sub>2</sub> FET is preceded by an ALD system (Savannah-100). The 2 nm thick HfO<sub>2</sub> layer is grown using pure water and Tetrakis (dimethylamino) hafnium as the precursor at  $200$   $^{\circ}\text{C}$  and 20 ALD cycles. Phototransistor performances were measured using a probe station connected to a Keithley 4200 semiconductor characterization system at room temperature. A 405 nm laser was used as incident light. For the conditions of the oscilloscope used in the measurements, we adapt an oscilloscope (type UTD2202CE, 200 MHz, UNI-T ltd, China) to characterize the acquired electrical pulsed message, and the rising time and falling time of the response curve can be accurately determined at the frequency of 500 Hz.

## RESULTS AND DISCUSSION

**Growth and Characterization of SnS<sub>2</sub> Nanoflakes.** SnS<sub>2</sub> nanoflakes were prepared by a modified CVD system with four temperature zones, which were specially designed and schematically illustrated in Figure 1a. Sulfur powders located in the first temperature zone at  $120$   $^{\circ}\text{C}$  and SnI<sub>2</sub> powders located in the second temperature zone at  $280$   $^{\circ}\text{C}$  were used as source materials. In these two zones, sulfur powders gasify

quickly while SnI<sub>2</sub> powder gasifies gradually. Then the gaseous sulfur and gaseous SnI<sub>2</sub> were transferred to the third temperature zone by carrier Ar gas. The third temperature control zone with a temperature of  $650$   $^{\circ}\text{C}$  was used as the reaction zone to make sure the source materials were reacting completely. In this zone, gaseous state SnI<sub>2</sub> and sulfur produces chemical reaction generated gaseous I<sub>2</sub> and SnS<sub>2</sub>. In order to avoid the generation of a sulfur vacancy ( $V_S$ ), sulfur must be superfluous. In general, the existence of  $V_S$  will decrease the performance (containing on/off ratio and response rate) of the SnS<sub>2</sub>-based photodetector.<sup>15</sup> Si or other substrates are located at the fourth temperature control zone at a temperature of  $400$   $^{\circ}\text{C}$  to receive deposition of SnS<sub>2</sub> nanoflakes. In this zone, SnS<sub>2</sub> crystals were grown as 2D upright plate-like crystals on substrates, and I<sub>2</sub> was kept in the gaseous state with pumping by mechanical pump. In this CVD method, reaction and deposition are separate, and thus we can control the reaction and deposition temperature more precisely. The deposition zone with a lower temperature can obviously increase the deposition rate. In addition, lower temperature and superfluous sulfur could prevent the dissociation of solid SnS<sub>2</sub> because of the high temperature, and S depletion could result in the phase transition from SnS<sub>2</sub> to SnS.<sup>21</sup> Ar was used as carrier gas in the growth of the SnS<sub>2</sub> crystal, and the tube was under a vacuum at 30 Pa. More details can be found in the [Experimental Section](#). Figure 1b exhibits the photograph of Zone 4 with a temperature of  $400$   $^{\circ}\text{C}$  and typical sample wafer, the yellow area signifies the existence of SnS<sub>2</sub> flakes with high-density and high production.

Figure 1c shows the scanning electron microscopy (SEM) image and enlarged SEM image of SnS<sub>2</sub> nanoflakes grown on Si substrate. It can be observed that plenty of vertical SnS<sub>2</sub> nanoflakes were interlaced and shrouded on the substrate, having an average size of up to  $30$   $\mu\text{m}$ . The spatial distribution of these 2D crystals suggests that SnS<sub>2</sub> rapidly nucleated on Si substrates to improve the formation of high-density and large size SnS<sub>2</sub> nanoflakes, which may be due to the fact that the temperature of the substrates was  $400$   $^{\circ}\text{C}$ , which is much lower

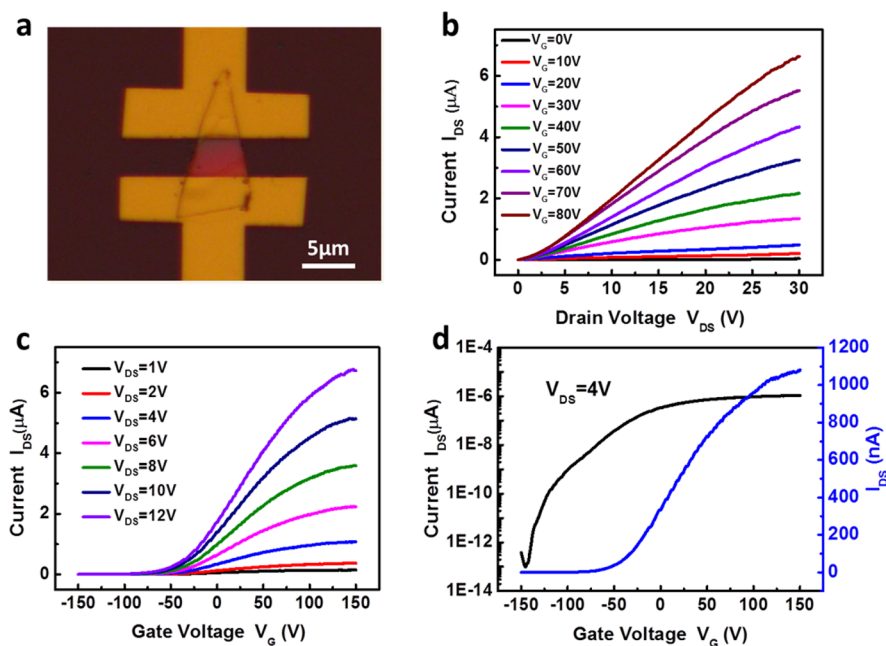


**Figure 3.** (a) SEM image of SnS<sub>2</sub> nanoflake based back-gated FET. (b) Output characteristics of the SnS<sub>2</sub> FET. (c) Transfer curve at different  $V_G$  and (d) transfer curve at  $V_{DS} = 4$  V of the FET.

than that previously reported (500–670 °C).<sup>13,15</sup> In particular, it can be seen from Figure 1d that some terraces exist on the surface of SnS<sub>2</sub> flakes, and such morphology with step-shaped terraces is further verified by AFM testing, as shown in Figure 1e, which is closely related to the screw-dislocation-driven spiral growth process of 2D SnS<sub>2</sub> crystals.<sup>4</sup>

We can see that the morphology of the as-grown SnS<sub>2</sub> flake is upright and interleaved with one another. The possible growth mechanism is that the deposition of SnS<sub>2</sub> is influenced by the existence of a dangling bond on the substrate surface that will cause a large migration barrier energy to restrict the in-plane growth of SnS<sub>2</sub> crystals. The in-plane growth is slower than upright growth due to the migration barrier of the dangling bond while the upright oriented SnS<sub>2</sub> nanoflake is larger than the in-plane oriented nanoflake. Alternatively, in spite of the difference in precursor, both of our products contain the SnS<sub>2</sub> phase that can easily introduce some defects inside or between the layers. The dislocations offer a bed for new branches of flake, and finally the SnS<sub>2</sub> flakes are found in any direction and of jigsaw pattern. Thus, the screw dislocation can lead to a spiral laminated structure on the surface and then the flake grows in a spiral manner in the direction of the Z axis.

Moreover, high-resolution TEM (HRTEM) and electron diffraction techniques are utilized to examine the microscopic structure of the 2D SnS<sub>2</sub> crystals. Figure 2a shows the HRTEM image of the as-grown SnS<sub>2</sub> nanoflake, indicating a high single-crystalline structure. From the HRTEM image, we can see that the measured interplanar distance of SnS<sub>2</sub> crystals is 0.318 nm and atoms arranged in the hexagonal pattern with interaxial angles of 120°. Figure 2b presents the selected area-electron-diffraction (SAED) pattern of an SnS<sub>2</sub> crystal, which clearly demonstrates single-crystal quality with the expected hexagonal crystal structure. All the characterization results confirm that high-quality SnS<sub>2</sub> were successfully synthesized by this modified CVD method. The SnS<sub>2</sub> nanoflakes are further characterized by Raman spectra, as shown in Figure 2c. The Raman spectrum of the as-prepared SnS<sub>2</sub> crystal shows a strong Raman peak at

313.3 cm<sup>-1</sup>, corresponding to the A<sub>1g</sub> phonon mode. In addition to the A<sub>1g</sub> mode, a weaker intralayer E<sub>g</sub> mode of the SnS<sub>2</sub> crystal with a peak at 203.3 cm<sup>-1</sup> is also observed.<sup>22</sup> The peak at 503 cm<sup>-1</sup> corresponded to the Si substrate.<sup>23</sup> Finally X-ray diffraction (XRD) measurement of the SnS<sub>2</sub> nanoflake is carried out to investigate the phase structure of the as-prepared SnS<sub>2</sub> sample, as shown in Figure 2d, which agreed well with the standard XRD spectra of a purely hexagonal SnS<sub>2</sub> (JCPDS PDF number 23-0677) crystal phase without any detectable impurities. These results further verify the high-quality crystalline structure of the as-synthesized products.

**SnS<sub>2</sub> Nanoflake-Based Field Effect Transistor.** The as-prepared SnS<sub>2</sub> nanoflakes were transferred to the Si substrate with a 300 nm SiO<sub>2</sub> layer and fabricated to the back-gated field effect transistor (FET) through an electron beam lithography (EBL) process, followed by the thermal deposition of Cr/Au (5 nm/50 nm, Cr used as an adhesion layer between Au and SiO<sub>2</sub>) electrodes. More details of the fabrication of SnS<sub>2</sub> nanoflake based FET can be found in the Experimental Section. Figure 3a shows the optical images of SnS<sub>2</sub>-nanoflake based FET, in which a single SnS<sub>2</sub> crystal flake, having an average thickness of 66.8 nm measured by atomic force microscopy, was used for the FET device. The output characteristic and transfer curves are shown in Figure 3b and c. As can be seen from the output curves, clear linear and saturation behavior are observed at low and high  $V_{DS}$ , respectively. To see the transfer characteristic more clearly, the transfer curve when the source-drain voltage was 4 V is shown in Figure 3d. By varying the  $V_{DS}$  from -150 to 150 V, the current changes from 10<sup>-13</sup> A to 10<sup>-6</sup> A, resulting in a high on/off ratio of 10<sup>7</sup>. The field effect mobility ( $\mu_e$ ) can be calculated using the following equation:

$$\mu_e = \frac{L}{WC_i V_{DS}} \times \frac{dI_{DS}}{dV_{GS}}$$

where  $L$  and  $W$  are the length and width of the FET, and herein  $L = 2$  μm and  $W = 5$  μm.  $C_i = 11.6 \times 10^{-4}$  nF·cm<sup>-2</sup> is the capacitance per unit area of the SiO<sub>2</sub> layer.<sup>21</sup> The estimated  $\mu_e$

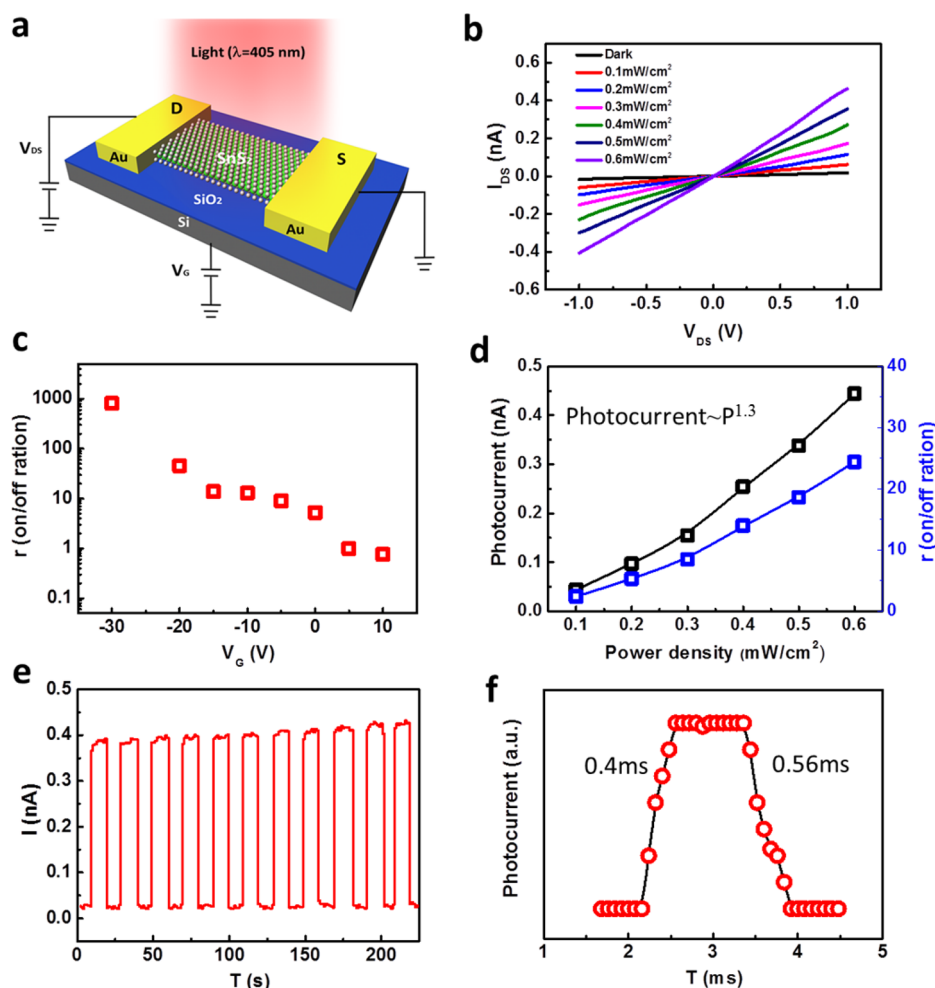


**Figure 4.** Performance measurement of the SnS<sub>2</sub>-based photodetector. (a) Schematic diagram of SnS<sub>2</sub> based photodetector. (b)  $I$ - $V$  curves of the photodetector under illumination with different power-densities. (c) Photocurrent and on/off ratio under illumination with different power-densities. (d) On/off ratio under  $V_G$  varied from  $-30$  to  $10$  V. (e) Cycling characteristics of the SnS<sub>2</sub>-based photodetector under the same incident light intensity of  $0.5 \text{ mW cm}^{-2}$ . (f) Rising curve and falling curve of the SnS<sub>2</sub>-based photoresponse.

is  $\sim 0.1 \text{ cm}^2 \cdot \text{V}^{-1} \text{ s}^{-1}$ . This relatively low mobility may be caused by the coulomb impurity scattering in the conventional back-gated FET, which may be derived from some factors, such as the oxidized surface layers of metal dichalcogenides during the ultrasonic dispersing process in the solution, surface defects, and surface adsorbed impurity. However, the low mobility can be improved by the enclosed layer in the surface of FET.

**Photoresponse Property of SnS<sub>2</sub>-Nanoflake-Based FET.** To detect the photoresponse property of the SnS<sub>2</sub>, lasers with  $\lambda = 405 \text{ nm}$  and power densities varying from  $0.1$  to  $0.6 \text{ mW cm}^{-2}$  were used as incident lights to excite a photocurrent of the SnS<sub>2</sub>-nanoflake-based FET. Figure 4a shows the schematic diagram of an SnS<sub>2</sub>-based photodetector. Figure 4b gives the  $I$ - $V$  curves under darkness and illumination with power densities varying from  $0.1$  to  $0.6 \text{ mW cm}^{-2}$ . The photocurrent remarkably increases with the enhancement of the incident light power, indicating that the device is a sensitive phototransistor. To clearly observe the increase of the photocurrent, the corresponding changes of photocurrent and on/off ratios with power densities of illumination from  $0.1$  to  $0.6 \text{ mW cm}^{-2}$  are discussed in Figure 4c and d. The on/off ratio can be calculated from the formula  $r = I_{\text{ph}}/I_{\text{dark}} = (I_{\text{light}} - I_{\text{dark}})/I_{\text{dark}}$ . The  $r$  can increase clearly even when the increase of light power density is only  $0.1 \text{ mW/cm}^2$ . And the  $r$  can reach up to

$24$  when the power density of incident light is only  $0.6 \text{ mW cm}^{-2}$ . Furthermore, the on/off ratio can enlarge immensely when the negative gate voltage is on-load on the transistor and decreased when the positive gate voltage is on-load on the transistor. As shown in Figure 4c, the on/off ratio increased from  $5$  to  $815$  when the voltage of the back gate ( $V_G$ ) was changed from  $0 \text{ V}$  to  $-30 \text{ V}$ . And when the  $V_G$  increased from  $0$  to  $10 \text{ V}$ , the on/off ratio decreased from  $5$  to  $0.76$ . Since the size of the phototransistor is about  $10 \mu\text{m}^2$ , the power density is from  $0.1$  to  $0.6 \text{ mW cm}^{-2}$ , the responsivity ( $R_\lambda$ ) and external quantum efficiency (EQE) were also calculated from the two formulas  $R_\lambda = I_{\text{ph}}/(P \times S)$  and  $\text{EQE} = hcR_\lambda/(e\lambda)$ . Here  $I_{\text{ph}}$  ( $V_{\text{DS}} = 1 \text{ V}$  and  $V_G = 0 \text{ V}$ ) is the photocurrent,  $P$  is the power density of incident light, and  $S$  is the effective illuminated area.  $h$  refers to the Planck's constant,  $c$  is the speed of light,  $\lambda$  describes the excitation light wavelength, and  $e$  is the elementary electronic charge. As a result,  $R_\lambda$  and the EQE are about  $5.3 \text{ A W}^{-1}$  and  $1626\%$ , respectively. Besides, specific detectivity ( $D^*$ ) is the reflection of the photodetector's sensitivity to detect weak optical signals, which can be calculated from the following formula:  $D^* = \frac{R_\lambda \sqrt{S}}{\sqrt{2eI_{\text{dark}}}}$ .<sup>16</sup> Here,  $R_\lambda$  is the responsibility that was calculated before, and thus the  $D^*$  was estimated to be  $1.1 \times 10^{10}$ . Figure 4e shows the cycling characteristics of the

Table 1. Photodetector Performance in This Work Compared with Those Reported by Others

device	rising time (ms)	falling time (ms)	responsivity ( $A W^{-1}$ )	EQE (%)	$D^*$ (Jones)	references
MoSe <sub>2</sub>	400	200	93.7			24
SnSe <sub>2</sub>	14.5	8.1	$1.1 \times 10^3$	$2.61 \times 10^5$	$1.01 \times 10^{10}$	25
WS <sub>2</sub>	5.3	5.3	$2.12 \times 10^{-5}$			26
GaTe	54	54	0.03	8		27
InSe	50	$4 \times 10^3$	12.3	1367	$10^{11}$	28
MoS <sub>2</sub>	0.07	0.11	0.57			29
graphene	$10^3$	$10^3$	0.18–1.75			30
black-P	1	1	$4.8 \times 10^{-3}$			31
SnS <sub>2</sub>	36	7	300	$4.65 \times 10^4$	$6 \times 10^9$	32
SnS <sub>2</sub>	$5 \times 10^{-3}$	$7 \times 10^{-3}$	$8.8 \times 10^{-3}$	2.4	$10^9$	13
SnS <sub>2</sub>	330	130	100	$3.3 \times 10^4$		14
SnS <sub>2</sub>	42	42	2			4
SnS <sub>2</sub>	20	16	260	$9.3 \times 10^4$	$1.9 \times 10^{10}$	16
SnS <sub>2</sub>	1	1	1.19			15
SnS <sub>2</sub>	0.4	0.56	354.4	$1.1 \times 10^5$	$2 \times 10^{10}$	This work

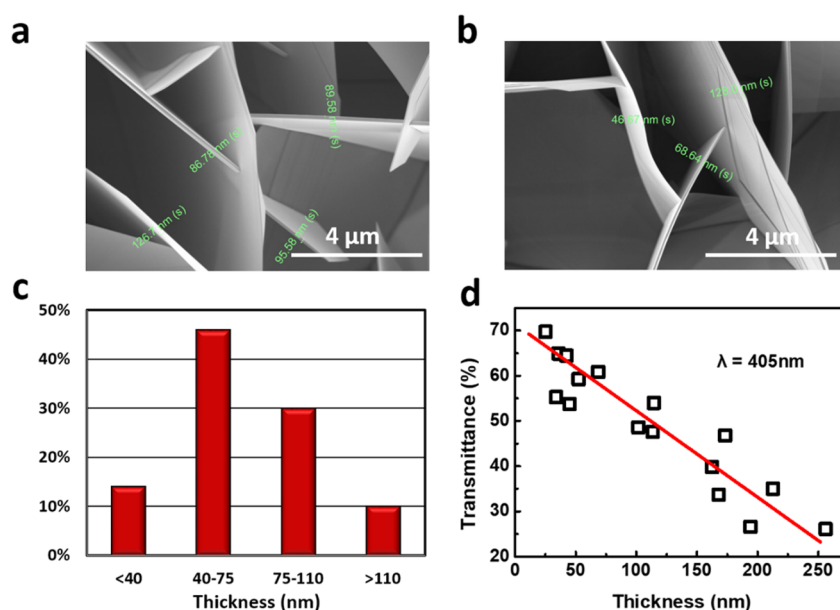


**Figure 5.** (a and b) Cross-sectional SEM images of as-grown SnS<sub>2</sub> flakes with thicknesses ranging from ~40 to ~120 nm. (c) Thickness distribution of as-grown SnS<sub>2</sub> nanoflake samples measured by AFM. (d) Transmittance change of SnS<sub>2</sub> nanoflakes with thicknesses varying from 25 to 256 nm at  $\lambda = 405$  nm.

photodetector for a long time under the same incident light intensity of  $0.5 \text{ mW cm}^{-2}$ . It is shown that the SnS<sub>2</sub>-based photodetector can stably respond to light. It is worth noting that the response times are quite fast and have exceeded the present installed measuring limit, and so we further measure the rising and falling times of the oscilloscope. As illustrated in Figure 4f, the rise time  $t_{\text{rise}} = 0.4$  ms, and the decay time  $t_{\text{decay}} = 0.56$  ms. The response rates obtained in this work can be comparable or even better than those of many recently reported 2D SnS<sub>2</sub> crystals or other 2D materials, as illustrated in Table 1. The observed fast photocurrent response rates, high responsivity, and external quantum efficiency can be attributed to the high single-crystal quality of the SnS<sub>2</sub> nanoflake verified by Raman, XRD, and TEM.

**Thickness-Dependent Photodetection Capability.** It is well-known that the thickness of the SnS<sub>2</sub> samples grown by the CVD method is not consistent. Different thicknesses of SnS<sub>2</sub> nanoflakes have significant influence on their photodetecting capability, but it has been rarely reported so far for

this reason that a lack in controllably high-production growth limits the selection of various SnS<sub>2</sub> samples. In this work, the high-production of the SnS<sub>2</sub> nanoflake samples provides more choices to different thicknesses of SnS<sub>2</sub> nanoflake samples. We find different cross-sectional thicknesses of vertical SnS<sub>2</sub> flakes from high-resolution SEM in Figure 5a and b, ranging from ~40 nm to ~120 nm. After measuring and classifying the thickness of these as-selected samples through atomic force microscopy (AFM), their statistic distribution diagram is shown in Figure 5c, in which an average thickness for most of the as-grown SnS<sub>2</sub> nanoflakes is in the range from 40 to 110 nm. In addition, with an increase of flake thickness, the light transmittance decreased linearly, indicating that the photon absorption coefficient or external efficiency has basically a positive linear relationship with flake thickness from 25 to 256 nm, as shown in Figure 5d.

Subsequently, a detailed measurement of the photodetecting property of SnS<sub>2</sub> nanoflakes with different thicknesses was carried out. As shown in Figure 6a, we find that the responsivity

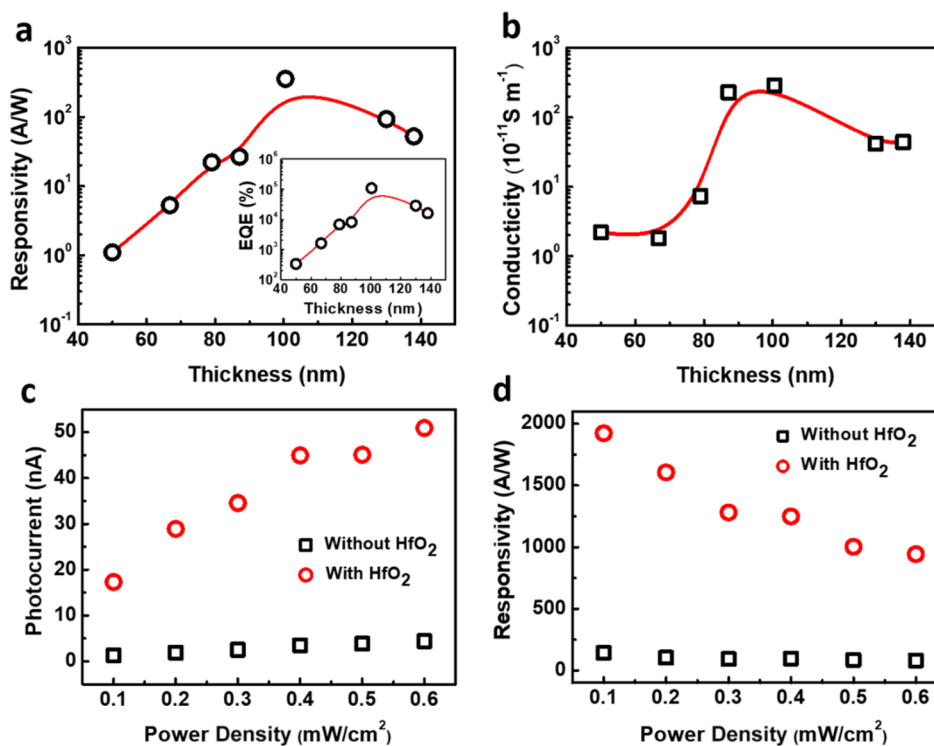


**Figure 6.** (a) Thickness-dependent responsivity of SnS<sub>2</sub> nanoflakes, in which an inset is a corresponding variation trend of EQE. (b) Conductivity change of SnS<sub>2</sub> nanoflakes with different thicknesses. (c) Photocurrent and (d) responsivity change of SnS<sub>2</sub> nanoflake-based photodetector with and without the sensitization process using 2 nm HfO<sub>2</sub>.

is strongly dependent on the average thicknesses of the SnS<sub>2</sub> nanoflake. With the increase of flake thickness from 50 to 100.5 nm, the responsivity rose dramatically by about 2 orders of magnitude. Correspondingly, the QE have shown the same trend as shown in the inset of Figure 6a. Note that the responsivity and QE can reach up to 354.4 A W<sup>-1</sup> and 1.1 × 10<sup>3</sup> % at a thickness of 100.5 nm, respectively, which can rival or surpass the reported SnS<sub>2</sub> or other 2D material-based photodetectors shown in Table 1. To further study the dependence relationship of photoelectron QE on flake thickness, we characterized the transmittance of few layered or multilayered SnS<sub>2</sub> flakes varying from 25 to 256 nm in thickness with a 405 nm incident light, as well as the dark conductivity, as shown in Figure 5d. When the thickness varies from 50 to 140 nm, the dark conductivity, as shown in Figure 4d, has a nonlinear dependence on the thickness. First the dark conductivity increases dramatically by more than 2 orders of magnitude to a climax at about 90 nm and then falls slowly, finally reaching a steady trend, which is similar to that in Figure 6b. It has been demonstrated that the band gap of SnS<sub>2</sub> changes little when the layer number increases from 83 to 240, corresponding to flake thicknesses varying from 50 to 140 nm, and then carrier density fluctuation induced by the thickness change is very small.<sup>33</sup> As a result, the change of the conductivity with the thickness actually reflects the change of carrier mobility ( $\mu_c$ ).

As is currently known, the photocurrent gain is strongly related to carrier mobility.<sup>34</sup> Under light illumination, the photocurrent gain  $G = \tau E (\mu_n + \mu_p) / L = \tau (1/t_{tn} + 1/t_{tp})$ , where  $L$  is distance between source and drain,  $\tau$  is life of carriers,  $\mu_n$  and  $\mu_p$  are mobility of electronics and holes,  $t_{tn} = L/\mu_n E$  and  $t_{tp} = L/\mu_p E$  are electronics and holes' traveling time between the source and drain electrodes, respectively. Generally, we

demonstrated that the influence of the nanoflake thickness below 95 nm on the detector responsivity originated from a combination of the enhanced absorption coefficient and the increased carrier mobility. However, when the nanoflake thickness is higher than 100.5 nm, the responsivity and dark conductivity show a downward or steady trend. On the one hand, the dark conductivity curve indicates that the carrier mobility tends to be stable as the flake grows thicker. On the other hand, we suppose that the downward trend of the responsivity curve is caused by the diminishment of the surface charge effect.<sup>35</sup>

We have proven that the as-fabricated SnS<sub>2</sub> nanoflake crystal is of high quality, as testified to by the high resolution TEM in Figure 2, and the intrinsic conductivity of the nanoflake is very low so that it is very easy to cause a charge trapping effect. In spite of that, there are some defects or oxides existing on the sample surface that serve as charge-trapping centers to capture free carriers excited by lattice thermal vibration, the electric field, or photonics. It is well-known that the surface or space charges have a density positively proportional to the free carrier density.<sup>35</sup> The charge effect influences the conductivity by two approaches. On the one hand, when the free carriers are trapped, extra electronics will be injected from the source to the semiconductor to neutralize the excess hole, and then the current as a whole will be increased. On the other hand, the surface or space charge will form an equivalent electric field that will excite more free carriers in return. According to the Mott–Gurney law,<sup>36</sup> the charge affected current  $J = \frac{9\epsilon_s \mu V^2}{8L^3}$ , where  $\epsilon_s$  is the surface permittivity, and  $V$  is the voltage. The thinner the nanoflake is, the higher the frequency of the carriers hitting and being captured by the trapping center becomes. When the nanoflake grows thick, both specific surface areas and the

influence of charge effect will decrease. As a result, when the flake thickness is higher than 100.5 nm, the conductivity and photo responsivity show a downward trend and finally reach a steady trend.

To carefully demonstrate the surface charging effect, we adopt a sensitized treatment for the SnS<sub>2</sub> surface using a 2 nm thick HfO<sub>2</sub> film with a high permittivity grown by atomic layer deposition (ALD), compared with the SnS<sub>2</sub> sample without sensitized treatment under the same conditions, as shown in Figure 6c and d. The thickness of the tested SnS<sub>2</sub> nanoflake is ~110 nm, where the influence of the surface charge effect was tested to be low. We speculate that HfO<sub>2</sub> sensitization on the surface will enhance the carrier trapping capacity as well as charge effect. Figure 6c and d shows that the photocurrents and photoresponsivity of the sensitized SnS<sub>2</sub> under the incident light power from 0.1 to 0.6 mW/cm<sup>2</sup> were increased by more than 10 times higher than those without HfO<sub>2</sub> thin film on the surface. The responsivity and EQE of the HfO<sub>2</sub> sensitized flake reached up to 1922 A W<sup>-1</sup> and 5.9 × 10<sup>5</sup> % at a power of 0.1 mW cm<sup>2</sup>, respectively. We can see clearly that the influence of the power density on the photocurrent and responsivity of sensitized nanoflakes shows the same trend as those of the raw nanoflake. The experimental results of high K material sensitized multilayered nanoflakes agree well with our conjecture. However, under the enhanced surface charging effect, majority carriers are directly excited by the space electric field, which takes place and disappears much more slowly. After the sensitization, the decay time increased from less than 1 ms to 5 ms, and the on/off ratio decreased remarkably due to the increase of dark current.

## CONCLUSION

We developed a simple and fruitful recipe to synthesize SnS<sub>2</sub> nanoflakes using a one-step CVD method. Separate reaction and deposition zones may effectively increase the deposition efficiency of high-quality crystals and assist in precisely understanding the growth and deposition temperature of SnS<sub>2</sub>. By transferring the SnS<sub>2</sub> nanoflakes onto SiO<sub>2</sub>/Si substrates and fabricating them to FET, high current on/off ratio FET and highly sensitive phototransistors were obtained. The SnS<sub>2</sub>-based photodetector shows fast response rates (rising time of 0.4 ms and falling time of 0.56 ms), high responsivity, and external quantum efficiency. And we find that most of the thicknesses of the SnS<sub>2</sub> crystals are in the range of 40–110 nm, and the responsivity and EQE have a positive relationship to the thickness of the SnS<sub>2</sub> crystals. The responsivity can reach up to 354.4 A W<sup>-1</sup> and 1.1 × 10<sup>5</sup> % at a thickness of 100.5 nm. After the sensitization using the HfO<sub>2</sub> nanolayer, the responsivity of the photodetector with a thickness of 130 nm can reach up to 1922 A W<sup>-1</sup>. The 2D SnS<sub>2</sub> based photodetectors may be used in optoelectronics applications.

## AUTHOR INFORMATION

### Corresponding Authors

\*E-mail: [jjli@iphy.ac.cn](mailto:jjli@iphy.ac.cn) (J.L.).

\*E-mail: [czgu@iphy.ac.cn](mailto:czgu@iphy.ac.cn) (C.G.).

\*E-mail: [tangcc@iphy.ac.com](mailto:tangcc@iphy.ac.com) (C.T.).

### ORCID

Ruhao Pan: 0000-0002-5573-2992

Yunze Long: 0000-0002-4278-4515

Junjie Li: 0000-0002-1508-9891

## Notes

The authors declare no competing financial interest.

## ACKNOWLEDGMENTS

The authors gratefully acknowledge financial support from the Ministry of Science and Technology of China (Grant No. 2016YFA0200800, 2016YFA0200400), the National Natural Science Foundation of China (Grant No. 11674387, 1170041373, 11704402, 61390503, 11574385, and 11574368), Key Research Program of Frontier Sciences of CAS (Grant No. QYZDJ-SSW-SLH042), and the “Strategic Priority Research Program” of CAS (Grant No. XDB07020200). The authors also thank Dr. Jinan Shi from the Advanced Materials Group of IOP-CAS for HRTEM characterization on the samples.

## REFERENCES

- (1) Novoselov, K. S.; Geim, A. K.; Morozov, S. V.; Jiang, D.; Zhang, Y.; Dubonos, S. V.; Grigorieva, I. V.; Firsov, A. A. Electric Field Effect in Atomically Thin Carbon Films. *Science* **2004**, *306*, 666–669. Huang, X.; Zeng, Z. Y.; Zhang, H. Metal dichalcogenide nanosheets: preparation, properties and applications. *Chem. Soc. Rev.* **2013**, *42*, 1934–1946. Liu, G. B.; Xiao, D.; Yao, Y. G.; Xu, X. D.; Yao, W. Electronic structures and theoretical modelling of two-dimensional group-VIB transition metal dichalcogenides. *Chem. Soc. Rev.* **2015**, *44*, 2643–2663.
- (2) Das, S.; Robinson, J. A.; Dubey, M.; Terrones, H.; Terrones, M. Beyond Graphene: Progress in Novel Two-Dimensional Materials and van der Waals Solids. *Annu. Rev. Mater. Res.* **2015**, *45*, 1–27.
- (3) Sharp, L.; Soltz, D.; Parkinson, B. A. Growth and Characterization of Tin Disulfide Single Crystals. *Cryst. Growth Des.* **2006**, *6*, 1523–1527.
- (4) Xia, J.; Zhu, D. D.; Wang, L.; Huang, B.; Huang, X.; Meng, X. M. Large-Scale Growth of Two-Dimensional SnS<sub>2</sub> Crystals Driven by Screw Dislocations and Application to Photodetectors. *Adv. Funct. Mater.* **2015**, *25*, 4255–4261.
- (5) Luo, B.; Fang, Y.; Wang, B.; Zhou, J. S.; Song, H. H.; Zhi, L. J. Two dimensional graphene–SnS<sub>2</sub> hybrids with superior rate capability for lithium ion storage. *Energy Environ. Sci.* **2012**, *5*, 5226–5230.
- (6) Seo, J. W.; Jang, J. T.; Park, S. W.; Kim, C.; Park, B.; Cheon, J. Two-Dimensional SnS<sub>2</sub> Nanoplates with Extraordinary High Discharge Capacity for Lithium Ion Batteries. *Adv. Mater.* **2008**, *20* (22), 4269–4273.
- (7) Zhang, Y. C.; Zhang, F.; Yang, Z. J.; Xue, H. G.; Dionysiou, D. D. Development of a new efficient visible-light-driven photocatalyst from SnS<sub>2</sub> and polyvinyl chloride. *J. Catal.* **2016**, *344*, 692–700.
- (8) An, X. Q.; Yu, J. C.; Tang, J. W. Biomolecule-assisted fabrication copper doped SnS<sub>2</sub> nanosheet–reduced graphene oxide junctions with enhanced visible-light photocatalytic activity. *J. Mater. Chem. A* **2014**, *2* (4), 1000–1005.
- (9) Song, H. S.; Li, S. L.; Gao, L.; Xu, Y.; Ueno, K.; Tang, J.; Cheng, Y. B.; Tsukagoshi, K. High-performance top-gated monolayer SnS<sub>2</sub> field-effect transistors and their integrated logic circuits. *Nanoscale* **2013**, *5*, 9666–9670.
- (10) Huang, Y.; Sutter, E.; Sadowski, J. T.; Cotlet, M.; Monti, O. L.A.; Racke, D. A.; Neupane, M. R.; Wickramaratne, D.; Lake, R. K.; Parkinson, B. A.; Sutter, P. Tin disulfide—An emerging layered metal dichalcogenide semiconductor: Materials properties and device characteristics. *ACS Nano* **2014**, *8*, 10743–10755.
- (11) Ou, J. Z.; Ge, W. Y.; Carey, B.; Daeneke, T.; Rotbart, A.; Shan, W.; Wang, Y. C.; Fu, Z. Q.; Chrimes, A. F.; Wlodarski, W.; Russo, S. P.; Li, Y. X.; Kalantar-zadeh, K. Physisorption-Based Charge Transfer in Two-Dimensional SnS<sub>2</sub> for Selective and Reversible NO<sub>2</sub> Gas Sensing. *ACS Nano* **2015**, *9*, 10313–10323.
- (12) Xu, K.; Li, N.; Zeng, D. W.; Tian, S. Q.; Zhang, S. S.; Hu, D.; Xie, C. S. Interface Bonds Determined Gas-Sensing of SnO<sub>2</sub>-SnS<sub>2</sub>

Hybrids to Ammonia at Room Temperature. *ACS Appl. Mater. Interfaces* **2015**, *7*, 11359–11368.

(13) Su, G. X.; Hadjiev, V. G.; Loya, P. E.; Zhang, J.; Lei, S. D.; Maharjan, S.; Dong, P.; Ajayan, P. M.; Lou, J.; Peng, H. B. Chemical vapor deposition of thin crystals of layered semiconductor SnS<sub>2</sub> for fast photodetection application. *Nano Lett.* **2015**, *15*, 506–513.

(14) Huang, Y.; deng, H.-X.; Xu, K.; Wang, Z.-X.; Wang, Q.-S.; Wang, F.-M.; Zhan, X.-Y.; Li, S. S.; Luo, J. W.; He, J.; Wang, F. Highly sensitive and fast phototransistor based on large size CVD-grown SnS<sub>2</sub> nanosheets. *Nanoscale* **2015**, *7*, 14093–14099.

(15) Yang, D.; Li, B.; Hu, C.; Deng, H.; Dong, D. D.; Yang, X. K.; Qiao, K. K.; Yuan, S. J.; Song, H. S. Controllable Growth Orientation of SnS<sub>2</sub> Flakes for Low-Noise, High-Photoswitching Ratio, and Ultrafast Phototransistors. *Adv. Opt. Mater.* **2016**, *4*, 419–426.

(16) Zhou, X.; Zhang, Q.; Gan, L.; Li, H. Q.; zhai, T. Y. Large-Size Growth of Ultrathin SnS<sub>2</sub> Nanosheets and High Performance for Phototransistors. *Adv. Funct. Mater.* **2016**, *26*, 4405–4413.

(17) Sun, Y. F.; Cheng, H.; Gao, S.; Sun, Z. H.; Liu, Q. H.; Liu, Q.; Lei, F. C.; Yao, T.; He, J. F.; Wei, S. Q.; Xie, Y. Freestanding tin disulfide single-layers realizing efficient visible-light water splitting. *Angew. Chem., Int. Ed.* **2012**, *51*, 8727–8731.

(18) Chia, X. Y.; Lazar, P.; Sofer, Z.; Luxa, J.; Pumera, M. Layered SnS versus SnS<sub>2</sub>: Valence and Structural Implications on Electrochemistry and Clean Energy Electrocatalysis. *J. Phys. Chem. C* **2016**, *120*, 24098–24111.

(19) Ham, G.; Shin, S.; Park, J.; Lee, J.; Choi, H.; Lee, S.; Jeon, H. Engineering the crystallinity of tin disulfide deposited at low temperatures. *RSC Adv.* **2016**, *6*, 54069–54075.

(20) Mutlu, Z.; Wu, R. J.; Wickramaratne, D.; Shahrezaei, S.; Liu, C.; Temiz, S.; Patalano, A.; Ozkan, C. S.; Lake, R. K.; Mkhoyan, K. A.; Ozkan, C. S. Phase Engineering of 2D Tin Sulfides. *Small* **2016**, *12*, 2998–3004.

(21) Zhou, T.; Pang, W. K.; Zhang, C.; Yang, J.; Chen, Z.; Liu, H. K.; Guo, Z. Enhanced Sodium-Ion Battery Performance by Structural Phase Transition from Two-Dimensional Hexagonal-SnS<sub>2</sub> to Orthorhombic-SnS. *ACS Nano* **2014**, *8*, 8323–8333.

(22) Smith, A. J.; Meek, P. E.; Liang, W. Y. Raman scattering studies of SnS<sub>2</sub> and SnSe<sub>2</sub>. *J. Phys. C: Solid State Phys.* **1977**, *10*, 1321–1323.

(23) Zi, J.; Büscher, H.; Falter, C.; Ludwig, W.; Zhang, K.; Xie, X. Raman shifts in Si nanocrystals. *Appl. Phys. Lett.* **1996**, *69*, 200–202.

(24) Jung, C.; Kim, S. M.; Moon, H.; Han, G.; Kwon, J.; Hong, Y. K.; Omkaram, I.; Yoon, Y.; Kim, S.; Park, J. Highly Crystalline CVD-grown Multilayer MoSe<sub>2</sub> Thin Film Transistor for Fast Photodetector. *Sci. Rep.* **2015**, *5*, 15313.

(25) Zhou, X.; Gan, L.; Tian, W.; Zhang, Q.; Jin, S.; Li, H.; Bando, Y.; Golberg, D.; Zhai, T. Ultrathin SnSe<sub>2</sub> Flakes Grown by Chemical Vapor Deposition for High-Performance Photodetectors. *Adv. Mater.* **2015**, *27*, 8035–8041.

(26) Perea-López, N.; Elías, A. L.; Berkdemir, A.; Castro-Beltrán, A.; Gutiérrez, H. R.; Feng, S.; Lv, R.; Hayashi, T.; López-Urías, F.; Ghosh, S.; Muchharla, B.; Talapatra, S.; Terrones, H.; Terrones, M. Photosensor Device Based on Few-Layered WS<sub>2</sub> Films. *Adv. Funct. Mater.* **2013**, *23*, 5511–5517.

(27) Wang, Z. X.; Safdar, M.; Mirza, M.; Xu, K.; Wang, Q. S.; Huang, Y.; Wang, F. M.; Zhan, X. Y.; He, J. High-performance flexible photodetectors based on GaTe nanosheets. *Nanoscale* **2015**, *7*, 7252–7258.

(28) Tamalampudi, S. R.; Lu, Y. Y.; Kumar, R. U.; Sankar, R.; Liao, C. D.; Moorthy, B. K.; Cheng, C. H.; Chou, F. C.; Chen, Y. T. High Performance and Bendable Few-Layered InSe Photodetectors with Broad Spectral Response. *Nano Lett.* **2014**, *14*, 2800–2806.

(29) Tsai, D. S.; Liu, K. K.; Lien, D. H.; Tsai, M. L.; Kang, C. F.; Lin, C. A.; Li, L. J.; He, J. H. Few-Layer MoS<sub>2</sub> with High Broadband Photogain and Fast Optical Switching for Use in Harsh Environments. *ACS Nano* **2013**, *7*, 3905–3911.

(30) Yu, X. C.; Dong, Z. G.; Liu, Y. P.; Liu, T.; Tao, J.; Zeng, Y. Q.; Yang, J. K. W.; Wang, Q. J. A high performance, visible to mid-infrared photodetector based on graphene nanoribbons passivated with HfO<sub>2</sub>. *Nanoscale* **2016**, *8*, 327–332.

(31) Buscema, M.; Groenendijk, D. J.; Blanter, S. I.; Steele, G. A.; van der Zant, H. S. J.; Castellanos-Gomez, A. Fast and broadband photoresponse of few-layer black phosphorus field-effect transistors. *Nano Lett.* **2014**, *14*, 3347–3352.

(32) Zhou, X.; Gan, L.; Zhang, Q.; Xiong, X.; Li, H. Q.; Zhong, Z. Q.; Han, J. B.; Zhai, T. Y. High performance near-infrared photodetectors based on ultrathin SnS nanobelts grown via physical vapor deposition. *J. Mater. Chem. C* **2016**, *4*, 2111–2116.

(33) Gonzalez, J.; Oleynik, I. I. Layer-dependent properties of SnS<sub>2</sub> and SnSe<sub>2</sub> novel two-dimensional materials. *Phys. Rev. B: Condens. Matter Mater. Phys.* **2016**, *94*, 125443.

(34) Sze, S. M.; Ng, K. K. *Physics of Semiconductor Devices*, 3<sup>rd</sup> ed., Wiley: San Jose, 2006.

(35) Chen, M. K.; Wang, Y. F.; Shepherd, N.; Huard, C.; Zhou, J. T.; Guo, L. J.; Lu, W.; Liang, X. G. Abnormal Multiple Charge Memory States in Exfoliated Few-Layer WSe<sub>2</sub> Transistors. *ACS Nano* **2017**, *11*, 1091–1102.

(36) Moss, T. S., Ed. *Handbook on Semiconductors*; Elsevier: North-Holland, Amsterdam, 1980; Vols. 1–4.